An advanced method to design graded cylindrical scaffolds with versatile effective cross-sectional mechanical properties

K. Cheikho, Cédric P. Laurent, J.F. Ganghoffer

An advanced method to design graded cylindrical scaffolds with versatile effective cross-sectional mechanical properties

K. Cheikho[a,*], C. Laurent[a], J.F. Ganghoffer[a]

[a] *CNRS UMR 7239 LEM3 - Université de Lorraine, Nancy, France*
[*] *corresponding author*

Abstract

The selection of the most-suited bone scaffold for a given clinical application is challenging, and has motivated numerous studies. They are mostly based on the characterization of cellular structures, generated from the three-dimensional repetition of a unit cell. However, the interest of circular graded bone scaffolds has been emphasized since they facilitate nutrient transport from the periphery to the core of the scaffold. In the present contribution, we present an advanced and versatile method to design graded circular porous 2D structures based on the conformal mapping of unit cells. We propose a method to generate 3D porous scaffolds by a multilayer repetition of the circular cross-section, resulting in tunable anisotropy depending on the clinical application. We then analyze the link between the porosities of the obtained structures and their effective elastic mechanical cross-sectional properties, making use of a novel and computationally efficient method allowing exhaustive parametric studies. The comparison of various conformal transformations and unit cell designs emphasizes the extent of mechanical properties and porosities that may be reached for a given constitutive material, including non-standard mechanical properties that open large perspectives towards the development of self-fitting scaffolds.

Keywords: graded scaffolds; finite element method; open-cell structures; 3D printing; conformal mapping.

1. Introduction

The selection of a suited scaffold geometry constitutes a milestone in the process of bone regeneration in tissue engineering and regenerative medicine, since its morphological and mechanical properties condition cell colonization and bone tissue generation (Bobbert and Zadpoor, 2017; Zadpoor, 2015) and therefore its final clinical success. The list of key requirements to be satisfied for scaffolds in tissue engineering includes (but is not limited to) (i) the biocompatibility of its constitutive material (see (Qu et al., 2019) for a recent review) and its osteconductive or osteoinductive properties (Ghassemi et al., 2018) (ii) its three-dimensional (3D)morphological properties such as pore size (Cai and Xi, 2008; Murphy et al., 2010; Norato and Johnson, 2011; Oh et al., 2007; Torres-Sanchez et al., 2017), overall porosity (Bandyopadhyay et al., 2010; Torres-Sanchez et al., 2017) , pore interconnectivity (Jones et al., 2009; Moore et al., 2004), surface curvature (Bidan et al., 2012; Paris et al., 2017; Rumpler et al., 2008; Sanz-Herrera et al., 2009),pore shape or the distribution of porosities (Poh et al., 2019) (iii) its effective mechanical properties such as apparent stiffness or elastic moduli

(Gómez et al., 2016; Norato and Johnson, 2011) or fluid mass transport properties (Gómez et al., 2016). In terms of effective mechanical properties, it is generally admitted that the proposed scaffold must mimic as close as possible the original mechanical physiological functions of the bone tissue it aims to replace (Afshar et al., 2016). The target apparent properties are obviously strongly influenced by the anatomical location and the type of bone tissue (Torres-Sanchez et al., 2017), as well as by age (Boskey and Coleman, 2010; Currey, 2004; Patton et al., 2019) or by the presence of different pathologies.

There is obviously a close relationship between the architecture of the selected structure and the resulting mechanical properties, as largely reported previously (Gibson, 2005) : as a consequence, the development of this porous structure requires a compromise between the constitutive properties of the biomaterial, the morphology of its microstructure and its apparent mechanical properties. This has led to numerous studies in the past two decades, even though it has been stated for a long time that "*there is enough evidence to postulate that ideal scaffold architecture does not exist*" (Bohner et al., 2011). The challenge of designing the most-suited scaffold design for a given application has therefore gained a growing interest particularly thanks to the emergence of 3D printing or additive manufacturing techniques (see (Cheng et al., 2019; Su et al., 2021; Wang et al., 2020) for recent reviews), allowing to precisely manufacture geometries issued from Computer-Assisted Design (CAD) (Bahraminasab, 2020).

Pore size has obvious consequences on mass transport within the scaffold (Dias et al., 2012; Jungreuthmayer et al., 2009). It has been shown that a pore size of roughly $100\ \mu m$ is essential for the bone generation process to progress successfully, with a preferred pore size superior than $300\ \mu m$ (Hutmacher, 2000; Karageorgiou and Kaplan, 2005; Oh et al., 2007). This has led to the proposition of numerous scaffold designs, generally based on the 3D periodic repetition of a unit cell (Afshar et al., 2016; Deng et al., 2021; Dias et al., 2012; Lin et al., 2004; Liu et al., 2018a; Yoo, 2011; Zhu et al., 2018). Different pore shapes have therefore been compared (Guyot et al., 2014; Rumpler et al., 2008), without any clear consensus concerning which pore shape should be selected. The morphology of the microstructure also conditions the available surface for cell adhesion (Van Bael et al., 2012). Among the commonly adopted unit cells, Triply Periodic Minimal Surfaces (TPMS) has gained a specific interest due to their high surface to volume ratio and easy structural modulation (Afshar et al., 2016; Liu et al., 2018a; Melchels et al., 2010), and since it has been observed that concave surfaces are most suitable than convex ones (Bidan et al., 2012). In opposition with those periodic 3D architectures, it has been reported that scaffolds with pore size gradients offer better seeding efficiency than homogeneous scaffolds (Sobral et al., 2011), and that pore size gradients from the core to the periphery of cylindrical scaffolds enhanced diffusion of nutrients (Ahn et al., 2010). In this last study, *cone-shape channels* have been showed to particularly encourage mass transport in 2D and 3D scaffolds. It has been also noticed that non-regular scaffold architectures result in better distribution of loads within the scaffold structure (Wieding et al., 2014). Such observations have led to the proposition of different heterogeneous geometries with pore size gradients (Afshar et al., 2016; Khoda and Koc, 2013; Liu et al., 2018a; Melchels et al., 2010; Nowicki et al., 2016; Poh et al., 2019; Yoo, 2012; Zhou et al., 2020a) aiming at closer replicating the multifunctions of bone tissues (Limmahakhun and Yan, 2017). These designs are commonly referred to as *functionally graded scaffolds* (FGS). These FGS are generated from a heterogeneous spatial distribution of the parameters of the unit cell, and generally show gradients of pore size in the three directions of space (in the sense of a cartesian basis) for rectangular scaffolds. However, scaffolds are generally intended to be placed within cylindrical holes or through bony tunnels resulting from the surgical procedure (Berner et al., 2014; Deng et al., 2021; Hutmacher, 2000; Paris et al., 2017; Wang et al., 2018), and scaffolds exhibiting cylindrical external shapes may therefore be preferred to be used clinically or evaluated *in vivo*. Graded cylindrical scaffold designs offering pore size gradients from the core to the periphery to facilitate nutrients diffusion as emphasized previously (Ahn et al., 2010) have however rarely been proposed until very recently (Liao et al., n.d.; Limmahakhun et al., 2017). In those two studies, the parameters of a unit

cell have been distributed non-uniformly in the radial direction in order to obtain a radial gradient for cylindrical bone scaffold, and the corresponding scaffold mechanical properties have been determined experimentally. Alternatively, in other fields of engineering or physics, circular heterogeneous architectures have been analyzed in the framework of conformal transformations, resulting in radially graded architectures mimicking the natural structure of sunflowers (Drenckhan et al., 2004). While conformal mapping framework has been used to generate deployable structures (Ishida et al., 2015, 2014), this framework has never been used to generate circular scaffold geometries with non-uniform spatial distribution of pores.

For perfectly periodic structures, the effective mechanical properties of porous scaffolds can obviously be obtained by the use of homogenization techniques from the definition of the unit cell, resulting in the evaluation of permeability (Dias et al., 2012) or elastic properties (Lin et al., 2004). This has led to the emergence of various unit cell geometries issued from topological optimization techniques aiming at finding the best structure for a given clinical application (Lin et al., 2004). Noteworthy, such homogenization procedures have emphasized the large range of effective elastic properties of two-dimensional (2D) metamaterials that may be obtained from various unit cells (Karathanasopoulos et al., 2018), and the crucial role of Poisson's ratio on the metamaterial's bulk and shear response. Effective properties of periodic heterogeneous media may also result from the development of micromechanical models (Ganghoffer and Reda, 2021; Louna et al., 2019). Nevertheless, these techniques are so far limited to perfectly periodic structures, and do not permit to predict the mechanical properties of graded scaffolds. Alternatively, due to the exact definition of scaffold geometry issued from CAD, finite element (FE) approaches have been also largely used to predict the 3D mechanical properties of various scaffold designs, including graded scaffolds (Afshar et al., 2016; Kolken et al., 2020; Zhu et al., 2018). Such approaches are usually computationally costly and require the manual design of a CAD definition of the scaffold, which restrains the scope of exhaustive parametric studies of various microstructures. More recently, energy-based methods based on the identification of macroscopic energy density stored in the homogeneous media with the sum of microscopic energy density have allowed to efficiently compute effective properties of heterogeneous media (Ayad et al., 2020).

Consequently, the first objective of the present study is to present an advanced framework to design graded cylindrical scaffolds by mapping a perfectly periodic reference domain in 2D onto a circular domain. This procedure will be firstly described, and a simple method to obtain cylindrical 3D scaffolds will be then presented. Since the generation of 3D scaffolds from the definition of 2D cross-sections lies on the addition of vertical pillars, we hypothesize that the computation of mechanical properties in the longitudinal direction is reduced to the summation of the mechanical contribution of each pillar, and we therefore restrict the rest of the study to the 2D scaffold cross-section. Our second objective is to investigate the range of effective cross-sectional mechanical properties that may be obtained depending on the selected Unit Cell (UC) topology and the mapping parameters between initial and circular domains, by making use of a computationally efficient numerical method. This method will be briefly summarized, and then applied to compute the cross-sectional effective properties of various scaffold geometries with a fixed porosity. We conclude by discussing the versatility of the proposed method, and its potential application to various clinical application.

2. Materials and methods

2.1. Mapping a perfectly periodic domain onto circular cross-sections

The framework of conformal mapping has been extensively used in various fields in order to transform a domain using a change of space variables into the complex domain. These mappings transform a translational periodicity of the microstructure within a domain of finite size into a rotational periodicity of the mapped

microstructure within the transformed domain, and therefore allow the generation of various circular patterns (Drenckhan et al., 2004; Fong, 2019). Angles are locally preserved through such mappings, in such a way that material isotropy may be locally conserved (Liu et al., 2013). By applying a conformal transformation to a porous periodic structure, it is therefore possible to obtain structures showing pore size gradients by virtue of the non-uniform transformation while preserving the porosity of the global structure. This constitutes an alternative way to distribute the same amount of material within the structure, depending on the definition of the applied transformation.

As an illustration, in the present study, three types of transformations were considered from the definition of a given Unit Cell (UC). Firstly, porous structures were obtained by making use of a Periodic Transformation (hereafter noted *PT*), which basically consists in the periodic repetition of the UC as commonly proposed in former studies. Secondly, two conformal transformations enabling to map the PT onto a non-periodic circular pattern were used, namely a Circular Transformation (hereafter noted *CT*) and a pine cone-like transformation (hereafter named *PCT*). Denoting (x_0, y_0) the spatial coordinates in the UC domain, λ the side of the square UC, PT is obtained by simply repeating the UC respectively n_x and n_y times in both directions:

PT: $$x = x_0 \pm n_x \lambda \; ; \; y = y_0 \pm n_y \lambda \tag{1}$$

From the position (x,y) of a point in the periodic domain, the two transformations receive the following mathematical expressions as follows:

CT: $$X = e^{\frac{x}{\alpha_1}} \cos\left(\frac{2\pi}{\alpha_2} y\right) \; ; \; Y = e^{\frac{x}{\alpha_1}} \sin\left(\frac{2\pi}{\alpha_2} y\right) \tag{2}$$

PCT: $$X = e^{\frac{x+y}{\alpha_1}} \cos\left(\frac{\pi}{\alpha_2}(x-y)\right) \; ; \; Y = e^{\frac{x+y}{\alpha_1}} \sin\left(\frac{\pi}{\alpha_2}(x-y)\right) \tag{3}$$

wherein α_1 and α_2 are the parameters that define the radial repetition and the angular repetition respectively.

These three transformations applied on an UC made of a square cell (1mm in length) with a circular inclusion is illustrated in Fig.1. As visible on this figure, the resulting structure exhibit a heterogeneous distribution of pore sizes.

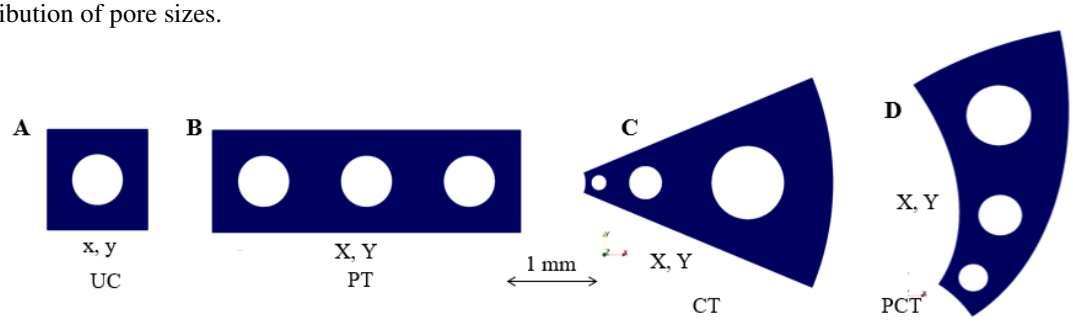

Fig. 1. Design of porous structures with the same overall porosity by making use of three different transformations, A. Unit Cell SC, B. Periodic transformation (PT), C. Circular Transformation (CT) and D. Pine Cone-Like Transformation. (PCT)

Applying such transformation to a periodic initial domain allows generating circular porous cross-sections with graded pore size from the core to the periphery of the structure, as illustrated in Fig.2 for an initial UC made of a square cell (1mm in length) with a square inclusion. To illustrate the versatility of the obtained

structures and associated effective properties, seven configurations were considered in the subsequent sections; such mappings are illustrated in Fig.2. While PT corresponds to a periodic transformation, CT1, CT2 and CT3 refer to to circular transformations and PCT1, PCT2 and PCT3 to pine cone-like transformations with $\alpha_1 = [2\pi/16, 2\pi/24, 2\pi/32]$ respectively. These transformations were applied based on various UC's that will be described later on.

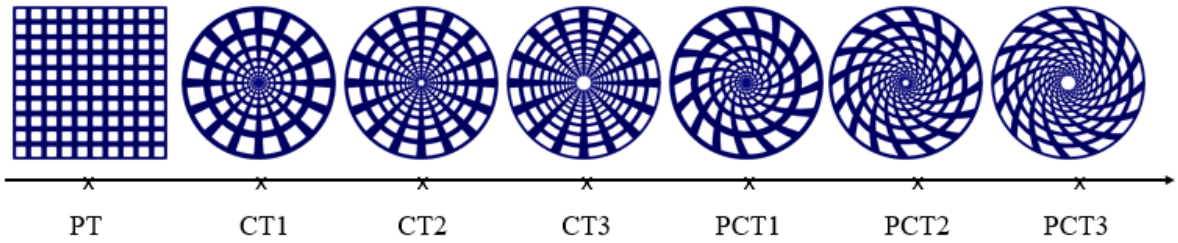

Fig. 2. Different transformations included in the parametric study, based on a square unit cell with a square shape inclusion.

2.2. Design of 3D scaffolds from 2D cross-sections

While the previous section described the design of 2D circular graded structures, scaffolds in tissue engineering obviously consists in open-cell 3D porous structures. In the literature, the three-dimensional porous scaffolds used to support tissue regeneration are derived from a periodic repetition of a unit cell in all three spatial directions, resulting in isotropic properties of the scaffold. The native bone tissue is however far from being isotropic (Li et al., 2013), and depending on the clinical application, anisotropic behavior may be suited (Rüegg et al., 2017). As a first and simple procedure to generate such 3D structures with tunable properties, we propose to periodically repeat the 2D sections obtained in the previous section with the addition of vertical pillars in the unit 3D cell, as illustrated in Fig. 3 for an initial square UC with a circular inclusion (45% overall porosity). Fig.3(A) illustrates the design of transversely isotropic scaffold for an initial periodic transformation (PT) of the UC in the transverse direction, while Fig.3(B) illustrates the associated circular graded 3D scaffold after a PCT transformation issued from equation 3.

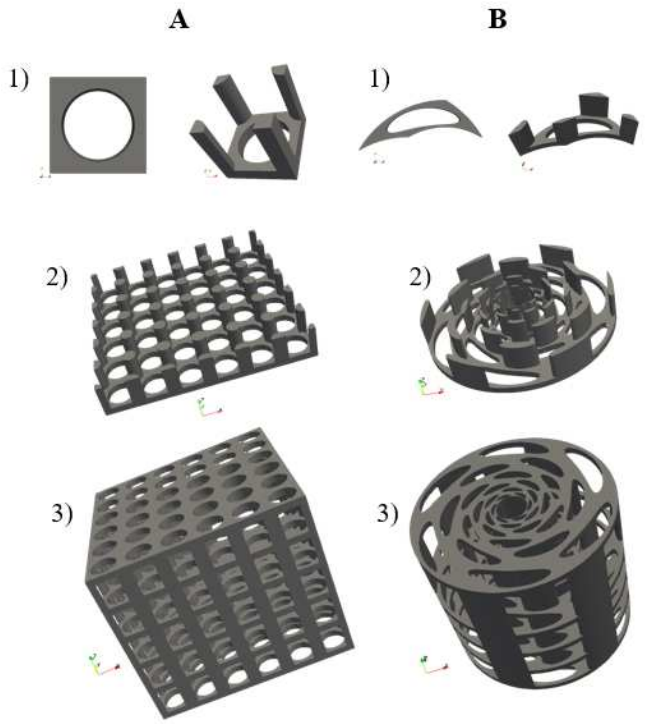

Fig. 3. Design of 3D open-cell scaffolds from the initial Unit Cell (UC). A. Periodic transformation of a square UC, with the addition of vertical pillars (1) in order to obtain 3D layers (2) to be repeated in the longitudinal direction so as to generate a transversely isotropic 3D scaffold (3). B. Pine-cone like transformation of a square UC, with the addition of vertical pillars (1) in order to obtain 3D layers (2) to be repeated in the longitudinal direction so as to generate a circular graded 3D scaffold (3).

The vertical pillars added to the UC follow the same transformation in the x-y plane than the UC. This method preserves the mechanical properties of pillars in the (Z) direction that may simply be deduced from the compressive behavior of these pillars. By controlling the initial cross-section of these pillars, the longitudinal mechanical properties of the scaffold may therefore be adjusted. Since the computation of the longitudinal mechanical properties is straightforward by a simple summation of the compressive response of each of these pillars, the next sections will be focused on the computation of cross-sectional properties that require some specific analysis.

2.3. Computation of apparent cross-sectional mechanical properties

The method described in 2.1 allows the design of numerous circular structures, whose resulting effective properties will obviously depend on the selected UC and the selected transformation. In this section, we describe how the effective properties of the 2D cross-sections were calculated in a computationally efficient way. This method is based on a variational approach and has been largely reported elsewhere in the framework of periodic homogenization (Ganghoffer and Reda, 2021) : we briefly describe below its application to the identification of effective properties of a heterogeneous structure.

Two distinct scales in the cross-section can be identified, *i.e.* the microscopic scale with microscopic position within the UC denoted y, and the macroscopic scale at the level of the entire domain. The balance of

linear momentum is written at the microlevel, considering that the constitutive material obeys a first gradient linear elasticity constitutive law given a static situation by:

$$\begin{aligned} &\boldsymbol{\sigma}\cdot\nabla_y+\mathbf{b}=0 \text{ in Y}\\ &\boldsymbol{\sigma}\cdot\mathbf{n}=\mathbf{t} \text{ on } \partial\text{Y}\\ &\boldsymbol{\sigma}=\ \mathbf{c}:\boldsymbol{\varepsilon} \end{aligned} \qquad (4)$$

with $\boldsymbol{\sigma}=\boldsymbol{\sigma}^T$ the symmetrical second-order Cauchy stress tensor, $\mathbf{b}$ the body forces that will be neglected later on, $\mathbf{n}$ the unit length exterior normal vector, $\mathbf{t}$ the traction vector and $\mathbf{c}$ the fourth-order microscopic rigidity tensor of the constitutive material of the scaffold.

A macroscopic strain $\boldsymbol{E}$ is imposed to the overall cross-section, and the displacement is decomposed into a linear function of the prescribed macroscopic strain and a fluctuation displacement $\tilde{u}_i(y)$. The fluctuating part of the displacement corrects for the existing discrepancies between the affine displacement of the Cauchy homogeneous continuum and the real displacement of the heterogeneous media. Therefore, the displacement and the micro-strain will express successively as follows:

$$u_i=E_{ij}\cdot y_j+\tilde{u}_i\left(y\right) \qquad (5)$$

$$\varepsilon_{ij}=E_{ij}+\tilde{\varepsilon}_{ij}\left(y\right) \qquad (6)$$

The fundamental assumption underlying the calculation of the effective mechanical properties towards the continuum problem is the principle of the equivalence of the macroscopic strain energy densities, the macroscopic energy density of the substitution medium being identified as the volume average of the microscopic energy density. This relation commonly called Hill-Mandel macrohomogeneity condition (Mindlin, 1964) is written as follows:

$$W_M(\mathbf{E})=\frac{1}{2}\left(E_{ij}:C^{\text{hom}}_{ijkl}:E_{kl}\right)=\left\langle w_m\left(\boldsymbol{\varepsilon}\right)\right\rangle_Y=\frac{1}{2}\left\langle\varepsilon_{ij}(y):c_{ijkl}:\varepsilon_{kl}(y)\right\rangle_Y \qquad (7)$$

With $\boldsymbol{Y}$ representing the entire domain of the structure.

The minimization principle of the energy amongst all admissible displacement fluctuations writes as follows:

$$W_M(\mathbf{E})=Min_{\tilde{u}}\left\langle w_m\left(\boldsymbol{\varepsilon}\right)\right\rangle=Min_{\tilde{u}}\frac{1}{2}\int_Y\left(E_{ij}+\nabla_{y_j}\tilde{u}_i\right):c_{ijkl}(y):\left(E_{mn}+\nabla_{y_n}\tilde{u}_m\right) \qquad (8)$$

To find the rigidity effective tensor of a given isotropic structure in two dimensions, two elastic parameters have to be identified and therefore two kinematic loadings must be applied. The rigidity tensor is then calculated from equation (8), from which we can deduce Young's modulus, Poisson's ratio, as well as the bulk and shear moduli. The applied kinematic loadings applied to structures with symmetries in translation (issued from the transformation PT) or in rotation (issued from the transformations CT or PCT) are illustrated

in Fig.4. They give access to the Young's modulus and shear modulus in the case of PT, or to the bulk and shear moduli in the case of CT and PCT. Obviously, from the identification of two elastic parameters, one can easily deduce another set of elastic isotropic parameters from classical relations of continuum mechanics.

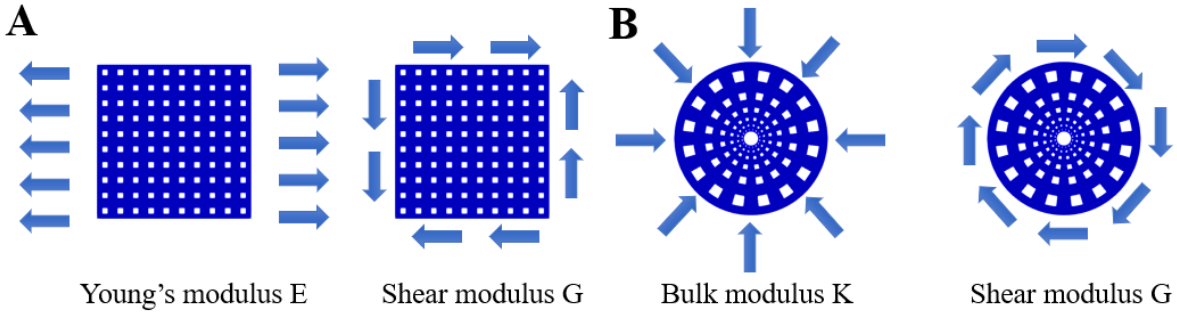

Fig. 4. Applied kinematic loadings for structures with symmetries (A) in translation and (B) in rotation.

For the structures with symmetries in the initial parent domain, a macroscopic transversal deformation is applied on the structure $E_{xx}=1$, that leads to identify $C_{11}=2\,W/V$, with W and $V$the strain energy and the volume of the heterogeneous structure respectively. A macroscopic biaxial deformation is applied on the structure $E_{xx}=1$ and $E_{yy}=1$, that leads to identify $C_{12}=(2\,W/V-C_{11}-C_{22})$.

For the structures with symmetries in rotation, a macroscopic compression deformation is applied on the structure $E_{rr}=1$, that leads to identify the apparent bulk modulus $K=W/2V$. A macroscopic torsion is applied on the structure, fixed in the center $E_{\theta\theta}=1$, that leads to identify the apparent shear modulus $G=2W/V$. K and G are calculated from the apparent compliance tensor using the relation as follows:

$$K=\frac{1}{S_{iikk}}\ \textit{and}\ G=\frac{1}{2S_{12}} \tag{9}$$

where S represents the compliance tensor.

In this work, we implement the previous procedure for the computation of effective 2D mechanical properties using the finite element code FreeFem++. The body forces in equation 4 being neglected, the Boundary Value Problem (BVP) is written as follows:

$$-\operatorname{div}\left\{c_{ijkl}(y):\left(E_{kl}+\nabla_{y_l}\left(H^{E}_{kmn}(y):E_{mn}\right)\right)\right\}=0 \tag{10}$$

In which divdenotes the divergence operator with respect to the microscopic coordinate and H^E is third-order localization tensor relating the microscopic displacement to the macroscopic strain. The kinematic loading was applied as illustrated in Fig.4, and we detail hereafter an example of the identification of $\mathbf{C}^{\text{hom}}$ for a structure with periodicity in translation (issued from PT).

Using the finite element code FreeFem++, the heterogeneous structure is meshed with linear triangular elements, and the evaluation of the localization operator by solving the BVP leads to the computation of the rigidity tensor C^{hom}_{ijkl} of the full structure. The effective elastic properties are calculated using the strain energy-based method, based on the relationship established between the strain energy of the microstructure and that of the homogenized equivalent model under specific boundary conditions. The numerical homogenization

technique consists in determining the overall effective Cauchy elastic coefficients over a representative unit cell, relying on a finite element discretization of the unit cell geometry (Goda and Ganghoffer, 2016, 2015).

For the calculation of the cross-sectional apparent properties of various structures, a polylactic acid (PLA) was selected ($E=1820MPa$, $\nu=0.3$, (Mirkhalaf and Fagerström, 2019)) as the constitutive material since it is widely used in the biomedical field and compatible with the fused-depositing modelling technique, which constitutes the most common and cheap 3D printing method to obtain scaffolds.

2.4. Selection of Unit Cells (UC) in the reference periodic domain

As an illustration of the versatility of the previous method of the calculation of the apparent mechanical properties and the large range of reachable apparent properties, six different types of UC were selected for the design of various scaffolds cross-sections. Firstly, classical pore shapes like a square cell in a circular inclusion (denoted *SC*), a square cell with a square inclusion (denoted *SS*) and a hexagonal cell (denoted *HX*) were selected (Rumpler et al., 2008). Less conventionally, auxetic cells (*i.e.* exhibiting negative Poisson's ratio) were selected due to their capacity to offer a large range of effective mechanical properties have been largely emphasized (Barchiesi et al., 2021; Karathanasopoulos et al., 2018; Kolken et al., 2020; Xin et al., 2020). Particularly, a pantograph-like UC (denoted *PT*) was selected due to its capacity to exhibit soft-modes (Barchiesi et al., 2021), for instance compression at low energy. Similarly, two types of hexachiral UC were selected since chiral structures are associated with easily tunable properties depending of the UC parameters (Xin et al., 2020). A classical hexachiral structure, exhibiting a "normal" auxetic mode (denoted *HCN*), was firstly selected. A degeneration of this UC into a non-chiral structure, therefore more "rigid" and denoted *HCR*, was secondly selected. These six types of UC are illustrated on Fig. 5 for various porosities. The geometrical parameters of these UC condition its overall porosity, and therefore different porosities were considered for each type of UC. Indeed, SC is dependent on the radius of its circular inclusion, SS is dependent on the length of its inner square inclusion, HX is dependent on the side length of its hexagonal inclusion, PT is dependent on the thickness of the ligaments and the length of the arc describing the inclusions, HCR is dependent on the length and thickness of its ligaments. The HCN unit cell is derived in two versions, HCN1 and HCN2, described by four parameters: the outer circle diameter, the inner circle diameter, and the thickness of its ligament. HCN1 refers to a hexachiral unit cell having tunable outer circle diameter, while HCN2 refers to a hexachiral unit cell having a tunable ligament thickness. For a given UC, defined through this set of parameters, the porosity was defined as the ratio of material with respect to a plain 1*1 mm square. The pore size was also computed, and defined as the maximal linear dimension of the hole for each UC.

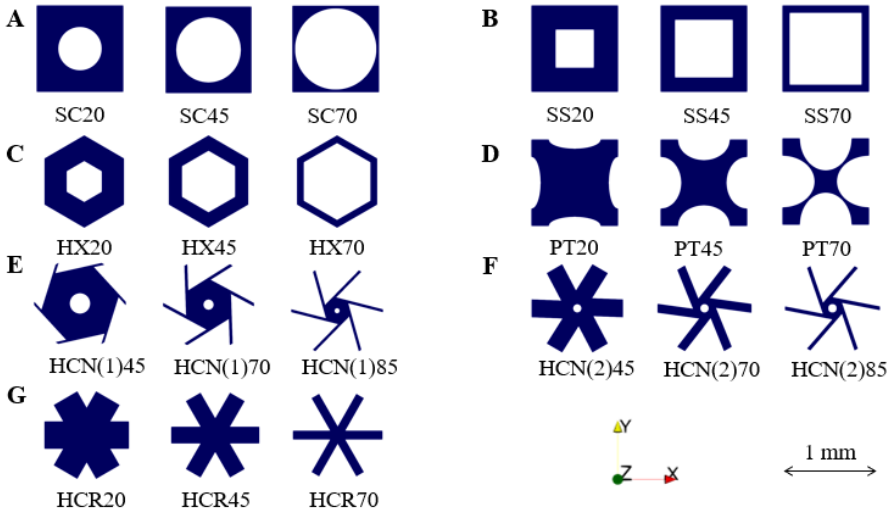

Fig. 5. Selected Unit Cells with various porosities. (A) Square cell with circular inclusion (B) Square cell with square inclusion (C) Hexagonal cell with hexagonal inclusion (D) Pantograph-like cell (E) and (F) "normal" hexachiral cells (G) "rigid" hexachiral cell. The legend below each geometry refers the abbreviation of the cell type and its porosity with respect to a plain 1*1 mm squared.

3. Results

3.1. Effect of the unit cell topology on morphological properties

As illustrated in Fig.6 for two particular types of UC and a periodic mapping of 10 x 10 UC, the apparent porosity of the generated structures largely depends on the parameters of the UC. The full range of porosities going from 0% to 100% are theoretically reachable, with obvious limitations concerning the printability of the structure that will be discussed later on.

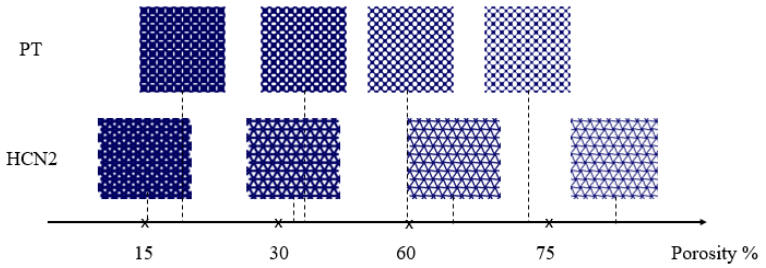

Fig. 6. Computed porosity of cross-sections for periodic repetitions of pantograph-like (PT) unit cell, and hexachiral (HCN2) unit cell.

Interestingly, the relation between apparent porosity and pore size largely depends on the selected UC, as emphasized in Fig. 7. For each of the six types of selected UC, pore sizes were computed for different apparent porosities resulting from a different set of parameters. Hexagonal structures (HX) offer the biggest pores for a given porosity, while hexachiral structure (HCN) offers the smallest pores. The parametrization of the pantograph-like structure results in a linear relation between porosity and pore size. To emphasize the pore size gradient from the core to the periphery of the proposed scaffolds, the pore size was computed (Fig. 8) as a

function of the radius for the transformation CT1 at a 64% of porosity for the 7 unit-cells illustrated in Fig. 5. Interestingly, while the relation was linear for SC, SS, HX and PT unit cells, the pore size non-linearly increased with radius for HCN1, HCN2 and HCR unit cells.

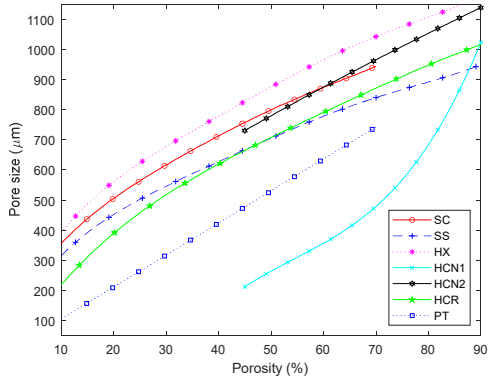

Fig. 7. Pore size in unit cell geometry as a function of the porosity.

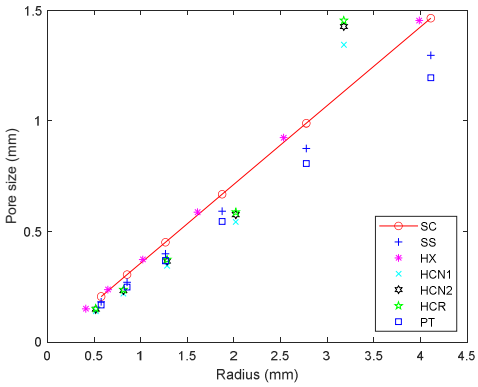

Fig. 8. Pore size as a function of the radius of the cylindrical scaffold created by CT1.

3.2. Effect of the unit cell topology on apparent properties

Apparent elastic mechanical properties were computed for various structures issued from PT, CT and PCT mappings using the numerical procedure described previously. An example of the finite element mesh for a CT mapping, as well as the computed displacement fields resulting from radial and tangential kinematic loadings to compute bulk and shear moduli respectively, are illustrated on Fig. 9.

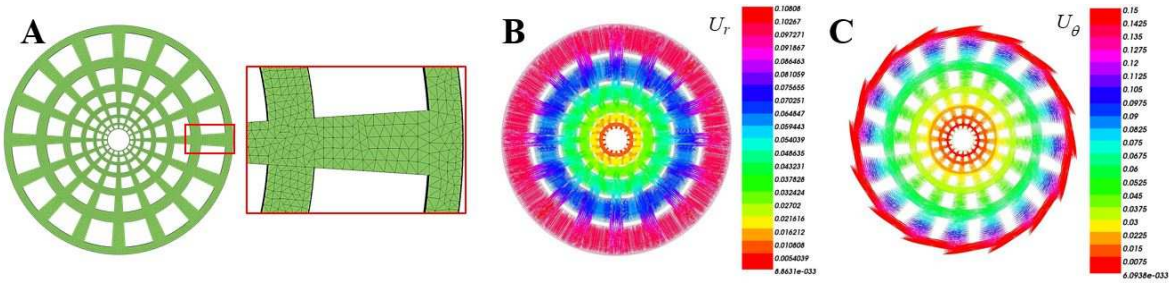

Fig. 9. Example of finite element mesh (A) and resulting radial displacement field for a radial kinematic loading (B) and tangential displacement field for a tangential kinematical loading (C), allowing to compute the bulk and shear moduli respectively.

The choice of the UC topology obviously influences the apparent properties that may be obtained, as emphasized previously (Karathanasopoulos et al., 2018). As an illustration, four different elastic properties in the macroscopic level (Young's modulus, Poisson's ratio, Bulk modulus and shear modulus) were computed as a function of the porosity using the numerical method detailed previously for different UC repeated

periodically (PT mapping with 10x10 repetitions) (Fig. 10), forming a porous structure with PLA as a constitutive material.

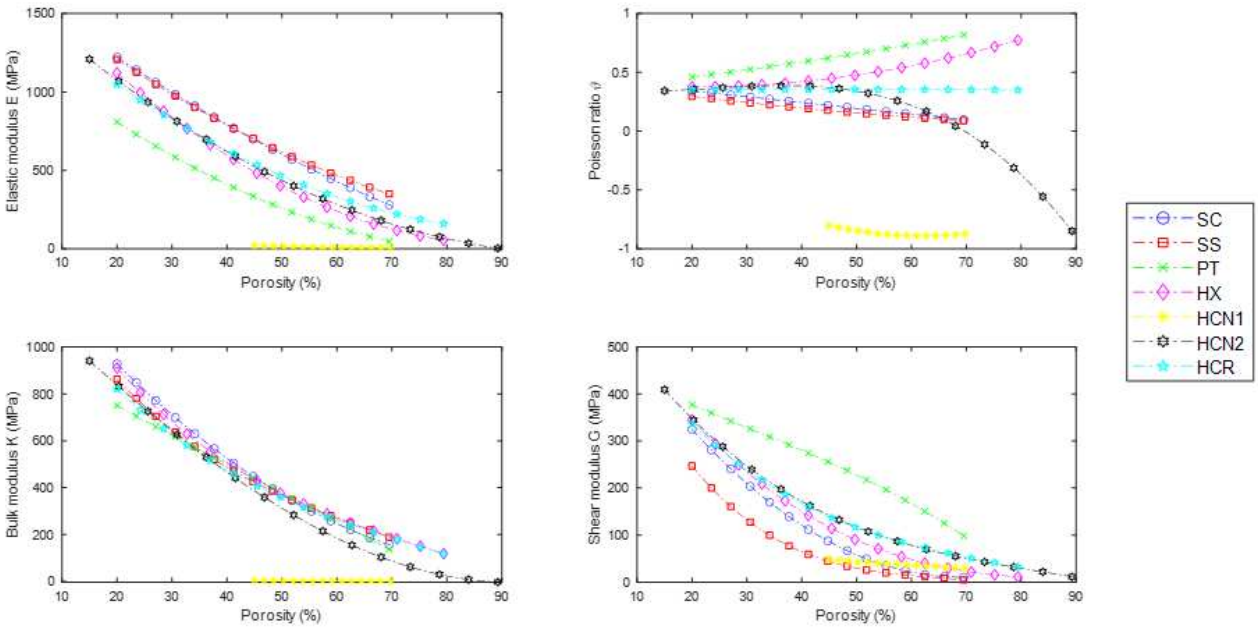

Fig. 10. Effect of the choice of Unit Cell (UC) on the relation between effective mechanical properties and porosity. These results are given for a periodic repetition of the UC (PT mapping) and PLA as a constitutive material.

The porosity – elasticity relationship is obviously nonlinear, is largely described for cellular solids (Gibson, 2005). Depending on the porosity, HCN1 and HCN2 may exhibit a clearly negative Poisson's ratio, as described previously (Xin et al., 2020), which results in a very low equivalent bulk and shear moduli compared to the other UC. The Poisson's ratio is a metric of the mechanical response since it uniquely controls the ratio of bulk to shear moduli. For a given porosity of 45%, the elastic modulus of structures with a SS unit cell is twice higher than the same structure with PT unit cell, while the Poisson's ratio is three times lower, and the bulk modulus remains roughly unchanged.

3.3. Effect of the type of transformations on the apparent scaffold mechanical properties

In the previous section, the effective mechanical properties of periodic structures based on different UC with different porosities were compared. This periodic repetition obviously results in square cross-sections with uniformly distributed pore sizes. In order to generate circular cross-sections with graded porous structure, CT and PCT mappings were applied to the periodic structures, and the resulting effective mechanical properties were computed as described previously. As a first example, Fig. 11 illustrates the various effective mechanical elastic properties in terms of Young's modulus, Poisson's ratio, bulk and shear moduli for the seven transformations showed previously (Fig. 2).

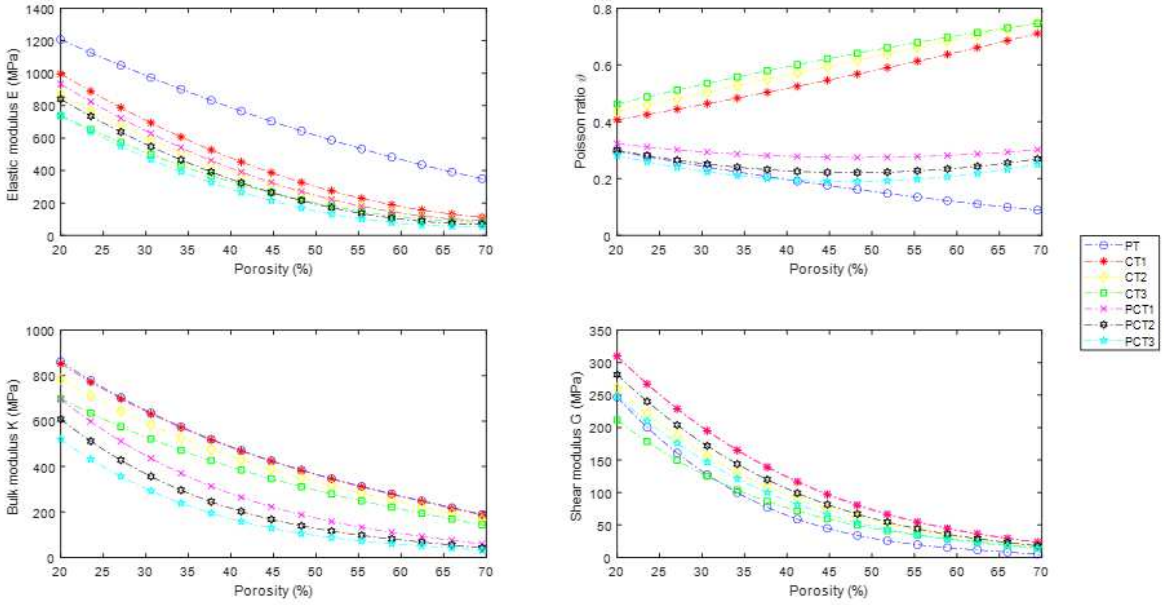

Fig. 11. Mechanical effective properties of the cross-sections issued from the transformations PT, CT1, CT2, CT3, PCT1, PCT2 and PCT3 of the unit cell SS.

Note worthy, for a given porosity, a classical periodic repetition of the SS unit cell gives higher bulk and Young's moduli than any other circular cross-section. For a given porosity of 45%, the Young's and bulk moduli are indeed more than three times higher for PT mapping than for PCT3 mapping. This is probably due to the chiral nature of the PCT transformation, which may involve a coupling between the bulk deformation and the folding of the structure as explained elsewhere (Meng et al., 2020).

A more exhaustive parametric study has been conducted by considering the seven transformations presented in section 2.1 and the seven UC presented in section 2.4 (leading to a total of 49 different cross-sections). The results of this parametric study in terms of effective elastic constants as a function of porosity are illustrated on Fig. 12, with still PLA as the same constitutive material. The versatility of the computed elastic properties is clearly emphasized, with Young's modulus reaching nearly zero for HCN1 unit cells ($E=19MPa$, corresponding to 1% of the constitutive material). Effective Poisson's ratios vary in the positive domain (0,1) except for the hexachiral UC, that result in a negative effective Poisson's ratio. A negative Poisson's ratio for cylindrical structures means that a compressive radial kinematical loading as illustrated in Fig.4(B) non-intuitively result in a tensile stress state within the cross-section.

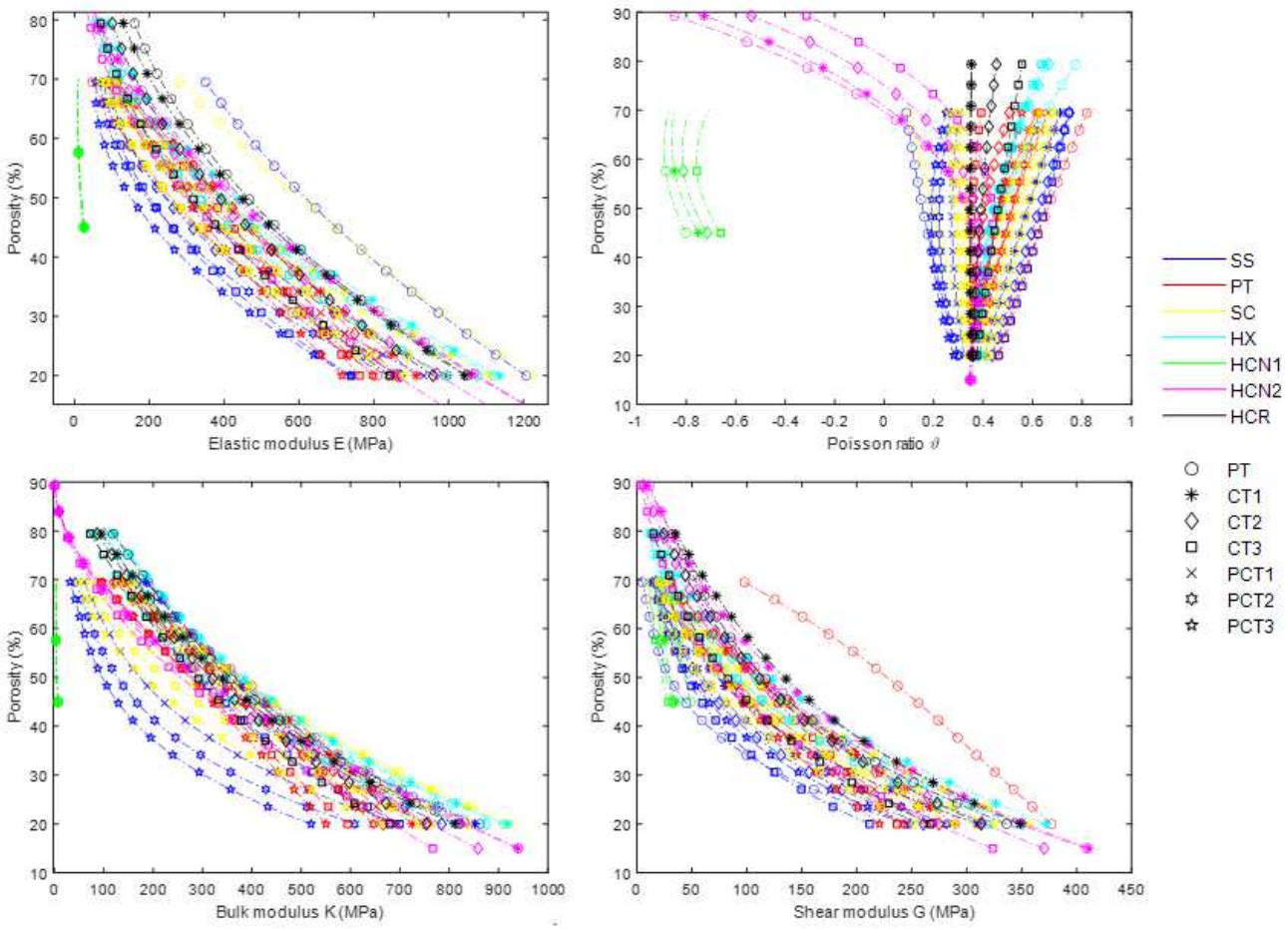

Fig. 12. Mechanical effective properties of the transformations PT, CT1, CT2, CT3, PCT1, PCT2 and PCT3 applied on the unit cells SC, SS, PT, HX, HCN1, HCN2 and HCR. The colors characterize the unit cell geometries and the marker symbols characterize the transformations.

4. Discussion and conclusion

Tremendous amount of studies has been devoted to bone scaffold design in the following two decades, since the identification of the most-suited structure for a given clinical application is challenging. Among these studies, the link between porosity and elastic properties has been largely explored, since bone regeneration requires both a high porosity with large pore size and sufficiently high mechanical properties. Obviously, changes in pore shape, porosity and pore size of a porous bone substitute affect its effective stiffness, which in return affects the contrast between the mechanical properties of the bone substitute and that of the surrounding bone tissue. The influence of the porosity on the effective mechanical properties have been largely reported previously (Bandyopadhyay et al., 2010; Karageorgiou and Kaplan, 2005; Poh et al., 2019), and non-linear relations on the form of power laws have been well described (Gibson, 2005). In such studies,

most of the reported 3D scaffolds are based on the 3D repetition of a Unit Cell (UC), mostly resulting in isotropic structures with homogeneous distribution of pores. However, initial bone tissue is far from being isotropic (Li et al., 2013), and specific clinical applications may require the development of anisotropic scaffolds (Rüegg et al., 2017). Moreover, there is a growing interest in the design and evaluation of graded bone scaffolds, due to the facilitated mass transport (Ahn et al., 2010) encouraging the cell colonization, the nutrient intakes, and the evacuation of the degradation products in the case of biodegradable scaffolds. Such gradients in pore size should be preferably orientated radially in circular structures, since most of the clinical procedures involve the filling of a bone tunnel, and thus the insertion of a cylindrical scaffold in contact with bone at its periphery. In the present contribution, we described a novel approach allowing to design circular anisotropic graded porous scaffolds with tunable properties. This method makes use of the concept of conformal transformation, which had never been applied to scaffold design to the best of author's knowledge. To illustrate the versatility of the reachable effective mechanical properties resulting from this method, we presented an exhaustive parametric study based on seven different UC and seven different transformations, including the periodic repetition of the UC that constitutes the gold standard in designing porous scaffolds. According to the selected type of UC and transformation, a large range of reachable cross-sectional mechanical properties were emphasized, including an auxetic behavior or nearly-soft modes in the radial direction. This versatility allows one to select the most appropriate structure for a given clinical application, depending on the desired porosity, pore size, and effective mechanical properties. To our knowledge, there are very few studies that discuss cylindrical scaffolds with radial pore size gradients from the core to the periphery. Ahn et al., 2010 presented such a geometry, but limited their work to the determination of the oxygen diffusion, emphasizing the interest of such gradients. They did not however reported mechanical properties to be compared with the results of the current study. On the contrary, several studies (Afshar et al., 2016; Liu et al., 2018b and Zhou et al., 2020b) reported linearly graded scaffolds issued from a linear variation of pore size distribution. For these structures, the resulting normalized Young's modulus E/E_0 (defined as the ratio between computed effective Young's modulus and the Young's modulus of the constitutive material) for a gradient of porosity going from 30% to 60% is ranged between the Young's modulus associated with the smallest and highest porosities. In this paper, our design allows us to get lower radial mechanical properties, with a potential application to minimally-invasive implantation through small bone tunnels. For instance, normalized Young's modulus obtained in the present study for a given porosity of 64.5% are ranged between $0.005 < E/E_0 < 0.25$ depending on the unit cell, while it ranged between $0.16 < E/E_0 < 0.4$ for perfectly periodic structures depending on the unit cell (Deng et al., 2021).In order to conduct such an exhaustive parametric study, an original numerical method was implemented in FreeFem++ based on the work from our team in the periodic homogenization framework, in which validations were already provided (Ayad et al., 2020; Ganghoffer and Reda, 2021; Goda et al., 2016; Karathanasopoulos et al., 2018). Based on a finite element discretization, the method was used to predict the 2D effective mechanical properties of the structure. Consequently, a simple procedure was presented to build 3D porous scaffolds from the layer-by-layer superposition of cross-section separated by pillars, the study was focused on the 2D properties of the scaffold cross-sections. Indeed, it was hypothesized that the longitudinal response of the generated 3D scaffolds was straightforward due to the simple geometry of the additional pillars. Similar studies may be anyway extended in 3D in the future following the same numerical procedure, in order to emphasize the large anisotropy that may be reachable for given UC and circular transformations. Our results indicated that this anisotropy may be particularly pronounced for auxetic UC's, since the computed cross-sectional bulk modulus was very low compared to the constitutive material's mechanical properties. This is the consequence of the fact that Poisson's ratio completely controls the ratio between bulk and shear moduli for an isotropic continuum (Karathanasopoulos et al., 2018). Consequently, by selecting an auxetic UC and rigid vertical pillars, the proposed approach may lead to the design of a cylindrical scaffold with a radial pore

size gradient, and with nearly-soft radial elastic properties compared to its axial properties. From a clinical point of view, this opens the possibility of designing self-fitting scaffolds that could be easily be compressed radially by the surgeon in order to enter a bone tunnel (Di et al., 2016). The ensuing deployment of the scaffold would thus contribute to its anchorage within the bone tunnel, with potential applications in the repair of cranial vault defects for instance (Berner et al., 2014; Lance and Wong, 2016). On the basis of the presented results, scaffolds based on the circular repetition of hexachiral unit cells appear to be the most suited for such an application from a mechanical point of view due to the associated low radial properties. Nevertheless, since no similar structure has been studied from a biological point of view to the best of our knowledge, the suitability of such pore size architecture for cellular adhesion and tissue growth should be assessed in the future to conclude to the relevance of this scaffold.

This principle could be extended in the future to the development of foldable and deployable scaffold designs applied to mini-invasive surgery as proposed recently (Bobbert et al., 2020; Di et al., 2016; Langford et al., 2021; Senatov et al., 2017; Wang et al., 2019), since similar structures have been proposed in the literature based on conformal transformations (Ishida et al., 2015, 2014). This would therefore require the extension of the proposed approach to large strains, and the study of buckling instabilities (Linn and Oliveira, 2017) that could appear in specific scaffold configurations due to the slenderness of some UC parts.

In the present contribution, we hypothesized that the resulting scaffold designs would be 3D-printed using one of the largely reported technique such as fused deposition modeling (Zein et al., 2002), and we therefore considered PLA as a potential constitutive material. It is obviously possible to imagine the realization of a bi-material structure that separates the properties of the pillars from those of the cross-sections, so as to extend the range of reachable effective properties. Nevertheless, the extent of possibilities on the approach is obviously limited by the capacity of the processing technique to precisely and faithfully manufacture the scaffold microstructure. Indeed, the pore size gradient from the core to the periphery using exponential mapping involves slender structures in the core of the scaffolds that could overcome the resolution of the process. However, recent advances in 3D-printing techniques make it possible to reach such resolution (Weisgrab et al., 2020), and the resulting effective mechanical properties have little dependence to these cells in the core of the scaffold. It is worth to stress out that, in addition to the macroscopic pores present in the proposed scaffold, novel techniques permitting the inclusion of microscopic porosities within the 3D printing filaments have been recently reported (Shalchy et al., 2020) and open even more perspectives towards the development of porous structures with multi-scale porosities.

As stated above, the effective mechanical properties were calculated using an efficient computational method, that allowed to present an exhaustive comparative study of various structures. Nevertheless, the question of the existence of closed-form solutions (that would not require any numerical modeling) for the effective homogeneous properties of the proposed structures is particularly interesting from a theoretical point of view. Indeed, the structures issued from the application of conformal mapping may approximated locally into affine transformations (Ostrosablin, 2006), raising the issue of a suited homogenization theory for quasi-periodic structures (Andrianov et al., 2006; Le and Marigo, 2018) and the question of the invariance of the boundary value problem of linear elasticity in the framework of conformal transformations (Lazar and Anastassiadis, 2008; Neff and Jeong, 2009).

Acknowledgements

The authors thank the French research agency (ANR) for the financial support provided by the ANR project “ArchiMatHos” devoted to metamaterials, as well as the INSIS-CNRS for their financial support concerning the field of *material by design*.

References

Afshar, M., Anaraki, A.P., Montazerian, H., Kadkhodapour, J., 2016. Additive manufacturing and mechanical characterization of graded porosity scaffolds designed based on triply periodic minimal surface architectures. Journal of the Mechanical Behavior of Biomedical Materials 62, 481–494.

Ahn, G., Park, J.H., Kang, T., Lee, J.W., Kang, H.-W., Cho, D.-W., 2010. Effect of pore architecture on oxygen diffusion in 3D scaffolds for tissue engineering. J Biomech Eng 132, 104506.

Andrianov, I.V., Awrejcewicz, J., Diskovsky, A.A., 2006. Homogenization of Quasi-Periodic Structures. Journal of Vibration and Acoustics 128, 532–534.

Ayad, M., Karathanasopoulos, N., Ganghoffer, J.F., Lakiss, H., 2020. Higher-gradient and micro-inertia contributions on the mechanical response of composite beam structures. International Journal of Engineering Science 154, 103318.

Bahraminasab, M., 2020. Challenges on optimization of 3D-printed bone scaffolds. BioMedical Engineering OnLine 19, 69.

Bandyopadhyay, A., Espana, F., Balla, V.K., Bose, S., Ohgami, Y., Davies, N.M., 2010. Influence of porosity on mechanical properties and in vivo response of Ti6Al4V implants. Acta Biomaterialia 6, 1640–1648.

Barchiesi, E., dell'Isola, F., Hild, F., 2021. On the validation of homogenized modeling for bi-pantographic metamaterials via digital image correlation. International Journal of Solids and Structures 208–209, 49–62.

Berner, A., Woodruff, M.A., Lam, C.X.F., Arafat, M.T., Saifzadeh, S., Steck, R., Ren, J., Nerlich, M., Ekaputra, A.K., Gibson, I., Hutmacher, D.W., 2014. Effects of scaffold architecture on cranial bone healing. International Journal of Oral and Maxillofacial Surgery 43, 506–513.

Bidan, C.M., Kommareddy, K.P., Rumpler, M., Kollmannsberger, P., Bréchet, Y.J.M., Fratzl, P., Dunlop, J.W.C., 2012. How Linear Tension Converts to Curvature: Geometric Control of Bone Tissue Growth. PLOS ONE 7, e36336.

Bobbert, F.S.L., Janbaz, S., van Manen, T., Li, Y., Zadpoor, A.A., 2020. Russian doll deployable meta-implants: Fusion of kirigami, origami, and multi-stability. Materials & Design 191, 108624. https://doi.org/10.1016/j.matdes.2020.108624

Bobbert, F.S.L., Zadpoor, A.A., 2017. Effects of bone substitute architecture and surface properties on cell response, angiogenesis, and structure of new bone. J. Mater. Chem. B 5, 6175–6192.

Bohner, M., Loosli, Y., Baroud, G., Lacroix, D., 2011. Commentary: Deciphering the link between architecture and biological response of a bone graft substitute. Acta Biomaterialia 7, 478–484.

Boskey, A.L., Coleman, R., 2010. Aging and bone. J Dent Res 89, 1333–1348.

Cai, S., Xi, J., 2008. A control approach for pore size distribution in the bone scaffold based on the hexahedral mesh refinement. Computer-Aided Design 40, 1040–1050.

Cheng, A., Schwartz, Z., Kahn, A., Li, X., Shao, Z., Sun, M., Ao, Y., Boyan, B.D., Chen, H., 2019. Advances in Porous Scaffold Design for Bone and Cartilage Tissue Engineering and Regeneration. Tissue Eng Part B Rev 25, 14–29.

Currey, J.D., 2004. Tensile yield in compact bone is determined by strain, post-yield behaviour by mineral content. Journal of Biomechanics 37, 549–556.

Deng, F., Liu, L., Li, Z., Liu, J., 2021. 3D printed Ti6Al4V bone scaffolds with different pore structure effects on bone ingrowth. Journal of Biological Engineering 15, 4.

Di, S., Liu, X., Liu, D., Gong, T., Lu, L., Zhou, S., 2016. A multifunctional porous scaffold with capacities of minimally invasive implantation, self-fitting and drug delivery. Materials Today Chemistry 1–2, 52–62.

Dias, M.R., Fernandes, P.R., Guedes, J.M., Hollister, S.J., 2012. Permeability analysis of scaffolds for bone tissue engineering. Journal of Biomechanics 45, 938–944.

Drenckhan, W., Weaire, D., Cox, S.J., 2004. The demonstration of conformal maps with two-dimensional foams. Eur. J. Phys. 25, 429–438.

Fong, C., 2019. Analytical Methods for Squaring the Disc. arXiv:1509.06344 [math].

Ganghoffer, J.F., Reda, H., 2021. A variational approach of homogenization of heterogeneous materials towards second gradient continua. Mechanics of Materials 158, 103743.

Ghassemi, T., Shahroodi, A., Ebrahimzadeh, M.H., Mousavian, A., Movaffagh, J., Moradi, A., 2018. Current Concepts in Scaffolding for Bone Tissue Engineering. Arch Bone Jt Surg 6, 90–99.

Gibson, L.J., 2005. Biomechanics of cellular solids. Journal of Biomechanics 38, 377–399.

Goda, I., Ganghoffer, J.-F., 2016. Construction of first and second order grade anisotropic continuum media for 3D porous and textile composite structures. Composite Structures 141, 292. https://doi.org/10.1016/j.compstruct.2016.01.061

Goda, I., Ganghoffer, J.-F., 2015. Identification of couple-stress moduli of vertebral trabecular bone based on the 3D internal architectures. Journal of the Mechanical Behavior of Biomedical Materials 51, 99–118. https://doi.org/10.1016/j.jmbbm.2015.06.036

Goda, I., Ganghoffer, J.-F., Czarnecki, S., Wawruch, P., Lewiński, T., 2016. Optimal internal architectures of femoral bone based on relaxation by homogenization and isotropic material design. Mechanics Research Communications 76, 64–71.

Gómez, S., Vlad, M.D., López, J., Fernández, E., 2016. Design and properties of 3D scaffolds for bone tissue engineering. Acta Biomaterialia 42, 341–350.

Guyot, Y., Papantoniou, I., Chai, Y.C., Van Bael, S., Schrooten, J., Geris, L., 2014. A computational model for cell/ECM growth on 3D surfaces using the level set method: a bone tissue engineering case study. Biomech Model Mechanobiol 13, 1361–1371.

Hutmacher, D.W., 2000. Scaffolds in tissue engineering bone and cartilage. Biomaterials, Orthopaedic Polymeric Biomaterials:

Applications of Biodegradables 21, 2529–2543.
Ishida, S., Nojima, T., Hagiwara, I., 2015. Design of Deployable Membranes Using Conformal Mapping. Journal of Mechanical Design 137.
Ishida, S., Nojima, T., Hagiwara, I., 2014. Mathematical Approach to Model Foldable Conical Structures Using Conformal Mapping. Journal of Mechanical Design 136.
Jones, A.C., Arns, C.H., Hutmacher, D.W., Milthorpe, B.K., Sheppard, A.P., Knackstedt, M.A., 2009. The correlation of pore morphology, interconnectivity and physical properties of 3D ceramic scaffolds with bone ingrowth. Biomaterials 30, 1440–1451.
Jungreuthmayer, C., Donahue, S.W., Jaasma, M.J., Al-Munajjed, A.A., Zanghellini, J., Kelly, D.J., O'Brien, F.J., 2009. A comparative study of shear stresses in collagen-glycosaminoglycan and calcium phosphate scaffolds in bone tissue-engineering bioreactors. Tissue Eng Part A 15, 1141–1149.
Karageorgiou, V., Kaplan, D., 2005. Porosity of 3D biomaterial scaffolds and osteogenesis. Biomaterials 26, 5474–5491.
Karathanasopoulos, N., Dos Reis, F., Reda, H., Ganghoffer, J.-F., 2018. Computing the effective bulk and normal to shear properties of common two-dimensional architectured materials. Computational Materials Science 154, 284–294.
Khoda, A.K.M.B., Koc, B., 2013. Functionally heterogeneous porous scaffold design for tissue engineering. Computer-Aided Design 45, 1276–1293.
Kolken, H.M.A., Lietaert, K., van der Sloten, T., Pouran, B., Meynen, A., Van Loock, G., Weinans, H., Scheys, L., Zadpoor, A.A., 2020. Mechanical performance of auxetic meta-biomaterials. Journal of the Mechanical Behavior of Biomedical Materials 104, 103658.
Lance, S., Wong, G., 2016. Resorbable Construct for Subtotal Cranial Vault Remodeling. Annals of Plastic Surgery 76, S196.
Langford, T., Mohammed, A., Essa, K., Elshaer, A., Hassanin, H., 2021. 4D Printing of Origami Structures for Minimally Invasive Surgeries Using Functional Scaffold. Applied Sciences 11, 332. https://doi.org/10.3390/app11010332
Lazar, M., Anastassiadis, C., 2008. Is incompressible elasticity a conformal field theory? Comptes Rendus Mécanique, Duality, inverse problems and nonlinear problems in solid mechanics 336, 163–169.
Le, D.T., Marigo, J.-J., 2018. Second order homogenization of quasi-periodic structures. Vietnam Journal of Mechanics 40, 325–348.
Li, S., Demirci, E., Silberschmidt, V.V., 2013. Variability and anisotropy of mechanical behavior of cortical bone in tension and compression. J Mech Behav Biomed Mater 21, 109–120.
Liao, B., Xia, R.F., Li, W., Lu, D., Jin, Z.M., n.d. 3D-Printed Ti6Al4V Scaffolds with Graded Triply Periodic Minimal Surface Structure for Bone Tissue Engineering. J. Mater. Eng. Perform.
Limmahakhun, S., Oloyede, A., Sitthiseripratip, K., Xiao, Y., Yan, C., 2017. Stiffness and strength tailoring of cobalt chromium graded cellular structures for stress-shielding reduction. Materials & Design 114, 633–641.
Limmahakhun, S., Yan, C., 2017. Graded Cellular Bone Scaffolds, Scaffolds in Tissue Engineering - Materials, Technologies and Clinical Applications. IntechOpen.
Lin, C.Y., Kikuchi, N., Hollister, S.J., 2004. A novel method for biomaterial scaffold internal architecture design to match bone elastic properties with desired porosity. Journal of Biomechanics 37, 623–636.
Linn, R.V., Oliveira, B.F., 2017. An analytical and numerical framework for evaluating axial compression of finite dimensional metallic foams by generalization of buckling effects. Mechanics of Advanced Materials and Structures 24, 1343–1352.
Liu, F., Mao, Z., Zhang, P., Zhang, D.Z., Jiang, J., Ma, Z., 2018. Functionally graded porous scaffolds in multiple patterns: New design method, physical and mechanical properties. Materials & Design 160, 849–860.
Liu, F., Mao, Z., Zhang, P., Zhang, D.Z., Jiang, J., Ma, Z., 2018b. Functionally graded porous scaffolds in multiple patterns: New design method, physical and mechanical properties. Materials & Design 160, 849–860. https://doi.org/10.1016/j.matdes.2018.09.053
Liu, Y., Liu, W., Su, X., 2013. Precise method to control elastic waves by conformal mapping. Theoretical and Applied Mechanics Letters 3, 021012.
Louna, Z., Goda, I., Ganghoffer, J.-F., 2019. Homogenized strain gradient remodeling model for trabecular bone microstructures. Continuum Mech. Thermodyn. 31, 1339–1367.
Melchels, F.P.W., Bertoldi, K., Gabbrielli, R., Velders, A.H., Feijen, J., Grijpma, D.W., 2010. Mathematically defined tissue engineering scaffold architectures prepared by stereolithography. Biomaterials 31, 6909–6916.
Meng, L., Shi, J., Yang, C., Gao, T., Hou, Y., Song, L., Gu, D., Zhu, J., Breitkopf, P., Zhang, W., 2020. An emerging class of hyperbolic lattice exhibiting tunable elastic properties and impact absorption through chiral twisting. Extreme Mechanics Letters 40, 100869.
Mindlin, R.D., 1964. Micro-structure in linear elasticity. Arch. Rational Mech. Anal. 16, 51–78.
Mirkhalaf, M., Fagerström, M., 2019. The mechanical behavior of polylactic acid (PLA) films: fabrication, experiments and modelling. Mechanics of Time-Dependent Materials In Press.
Moore, M.J., Jabbari, E., Ritman, E.L., Lu, L., Currier, B.L., Windebank, A.J., Yaszemski, M.J., 2004. Quantitative analysis of interconnectivity of porous biodegradable scaffolds with micro-computed tomography. J. Biomed. Mater. Res. 71A, 258–267.
Murphy, C.M., Haugh, M.G., O'Brien, F.J., 2010. The effect of mean pore size on cell attachment, proliferation and migration in collagen–glycosaminoglycan scaffolds for bone tissue engineering. Biomaterials 31, 461–466.
Neff, P., Jeong, J., 2009. A new paradigm: the linear isotropic Cosserat model with conformally invariant curvature energy. ZAMM - Journal of Applied Mathematics and Mechanics / Zeitschrift für Angewandte Mathematik und Mechanik 89, 107–122.
Norato, J.A., Johnson, A.J.W., 2011. A Computational and Cellular Solids Approach to the Stiffness-Based Design of Bone Scaffolds. J. Biomech. Eng.-Trans. ASME 133, 091003.

Nowicki, M.A., Castro, N.J., Plesniak, M.W., Zhang, L.G., 2016. 3D printing of novel osteochondral scaffolds with graded microstructure. Nanotechnology 27, 414001.

Oh, S.H., Park, I.K., Kim, J.M., Lee, J.H., 2007. In vitro and in vivo characteristics of PCL scaffolds with pore size gradient fabricated by a centrifugation method. Biomaterials 28, 1664–1671.

Ostrosablin, N.I., 2006. Affine transformations of the equations of the linear theory of elasticity. J Appl Mech Tech Phys 47, 564–572.

Paris, M., Götz, A., Hettrich, I., Bidan, C.M., Dunlop, J.W.C., Razi, H., Zizak, I., Hutmacher, D.W., Fratzl, P., Duda, G.N., Wagermaier, W., Cipitria, A., 2017. Scaffold curvature-mediated novel biomineralization process originates a continuous soft tissue-to-bone interface. Acta Biomaterialia 60, 64–80.

Patton, D.M., Bigelow, E.M.R., Schlecht, S.H., Kohn, D.H., Bredbenner, T.L., Jepsen, K.J., 2019. The relationship between whole bone stiffness and strength is age and sex dependent. Journal of Biomechanics 83, 125–133.

Poh, P.S.P., Valainis, D., Bhattacharya, K., van Griensven, M., Dondl, P., 2019. Optimization of Bone Scaffold Porosity Distributions. Sci Rep 9, 9170.

Qu, H., Fu, H., Han, Z., Sun, Y., 2019. Biomaterials for bone tissue engineering scaffolds: a review. RSC Adv. 9, 26252–26262.

Rüegg, J., Schumacher, R., Weber, F.E., Wild, M. de, 2017. Mechanical anisotropy of titanium scaffolds. Current Directions in Biomedical Engineering 3, 607–611.

Rumpler, M., Woesz, A., Dunlop, J.W.C., van Dongen, J.T., Fratzl, P., 2008. The effect of geometry on three-dimensional tissue growth. J R Soc Interface 5, 1173–1180.

Sanz-Herrera, J.A., Moreo, P., García-Aznar, J.M., Doblaré, M., 2009. On the effect of substrate curvature on cell mechanics. Biomaterials 30, 6674–6686.

Senatov, F.S., Zadorozhnyy, M.Yu., Niaza, K.V., Medvedev, V.V., Kaloshkin, S.D., Anisimova, N.Y., Kiselevskiy, M.V., Yang, K.-C., 2017. Shape memory effect in 3D-printed scaffolds for self-fitting implants. European Polymer Journal 93, 222–231.

Shalchy, F., Lovell, C., Bhaskar, A., 2020. Hierarchical porosity in additively manufactured bioengineering scaffolds: Fabrication & characterisation. Journal of the Mechanical Behavior of Biomedical Materials 110, 103968.

Sobral, J.M., Caridade, S.G., Sousa, R.A., Mano, J.F., Reis, R.L., 2011. Three-dimensional plotted scaffolds with controlled pore size gradients: Effect of scaffold geometry on mechanical performance and cell seeding efficiency. Acta Biomaterialia 7, 1009–1018.

Su, X., Wang, T., Guo, S., 2021. Applications of 3D printed bone tissue engineering scaffolds in the stem cell field. Regenerative Therapy 16, 63–72.

Torres-Sanchez, C., Al Mushref, F.R.A., Norrito, M., Yendall, K., Liu, Y., Conway, P.P., 2017. The effect of pore size and porosity on mechanical properties and biological response of porous titanium scaffolds. Materials Science and Engineering: C 77, 219–228.

Van Bael, S., Chai, Y.C., Truscello, S., Moesen, M., Kerckhofs, G., Van Oosterwyck, H., Kruth, J.-P., Schrooten, J., 2012. The effect of pore geometry on the in vitro biological behavior of human periosteum-derived cells seeded on selective laser-melted Ti6Al4V bone scaffolds. Acta Biomaterialia 8, 2824–2834.

Wang, C., Huang, W., Zhou, Y., He, L., He, Z., Chen, Z., He, X., Tian, S., Liao, J., Lu, B., Wei, Y., Wang, M., 2020a. 3D printing of bone tissue engineering scaffolds. Bioactive Materials 5, 82–91.

Wang, L., Qiu, Y., Lv, H., Si, Y., Liu, L., Zhang, Q., Cao, J., Yu, J., Li, X., Ding, B., 2019. 3D Superelastic Scaffolds Constructed from Flexible Inorganic Nanofibers with Self-Fitting Capability and Tailorable Gradient for Bone Regeneration. Advanced Functional Materials 29, 1901407.

Wang, S., Zhao, Z., Yang, Y., Mikos, A.G., Qiu, Z., Song, T., Cui, F., Wang, X., Zhang, C., 2018. A high-strength mineralized collagen bone scaffold for large-sized cranial bone defect repair in sheep. Regen Biomater 5, 283–292.

Weisgrab, G., Guillaume, O., Guo, Z., Heimel, P., Slezak, P., Poot, A., Grijpma, D., Ovsianikov, A., 2020. 3D Printing of large-scale and highly porous biodegradable tissue engineering scaffolds from poly(trimethylene-carbonate) using two-photon-polymerization. Biofabrication 12, 045036.

Wieding, J., Wolf, A., Bader, R., 2014. Numerical optimization of open-porous bone scaffold structures to match the elastic properties of human cortical bone. Journal of the Mechanical Behavior of Biomedical Materials 37, 56–68.

Xin, X., Liu, L., Liu, Y., Leng, J., 2020. 4D Printing Auxetic Metamaterials with Tunable, Programmable, and Reconfigurable Mechanical Properties. Advanced Functional Materials 30, 2004226.

Yoo, D., 2012. Heterogeneous minimal surface porous scaffold design using the distance field and radial basis functions. Medical Engineering & Physics 34, 625–639.

Yoo, D.J., 2011. Porous scaffold design using the distance field and triply periodic minimal surface models. Biomaterials 32, 7741–7754.

Zadpoor, A.A., 2015. Bone tissue regeneration: the role of scaffold geometry. Biomater. Sci. 3, 231–245.

Zein, I., Hutmacher, D.W., Tan, K.C., Teoh, S.H., 2002. Fused deposition modeling of novel scaffold architectures for tissue engineering applications. Biomaterials 23, 1169–1185.

Zhou, X., Jin, Y., Du, J., 2020. Functionally Graded Scaffolds with Programmable Pore Size Distribution Based on Triply Periodic Minimal Surface Fabricated by Selective Laser Melting. Materials 13, 5046.

Zhou, X., Jin, Y., Du, J., 2020b. Functionally Graded Scaffolds with Programmable Pore Size Distribution Based on Triply Periodic Minimal Surface Fabricated by Selective Laser Melting. Materials (Basel) 13, E5046. https://doi.org/10.3390/ma13215046

Zhu, L.-Y., Li, L., Shi, J.-P., Li, Z.-A., Yang, J.-Q., 2018. Mechanical characterization of 3D printed multi-morphology porous Ti6Al4V scaffolds based on triply periodic minimal surface architectures. Am J Transl Res 10, 3443–3454.